

Drastic Influence of Synthesis Conditions on Structural, Magnetic, and Magnetocaloric Properties of Mn(Fe,Ni)(Si,Al) Compounds

Nuendute, Balnude; Hanggai, Wuliji; Yibole, Hargen; Tana, Bao; Tegus, Ojiyed; Guillou, Francois

DOI

[10.3390/cryst12020233](https://doi.org/10.3390/cryst12020233)

Publication date

2022

Document Version

Final published version

Published in

Crystals

Citation (APA)

Nuendute, B., Hanggai, W., Yibole, H., Tana, B., Tegus, O., & Guillou, F. (2022). Drastic Influence of Synthesis Conditions on Structural, Magnetic, and Magnetocaloric Properties of Mn(Fe,Ni)(Si,Al) Compounds. *Crystals*, 12(2), Article 233. <https://doi.org/10.3390/cryst12020233>

Important note

To cite this publication, please use the final published version (if applicable). Please check the document version above.

Copyright


Other than for strictly personal use, it is not permitted to download, forward or distribute the text or part of it, without the consent of the author(s) and/or copyright holder(s), unless the work is under an open content license such as Creative Commons.

Takedown policy

Please contact us and provide details if you believe this document breaches copyrights. We will remove access to the work immediately and investigate your claim.

Article

Drastic Influence of Synthesis Conditions on Structural, Magnetic, and Magnetocaloric Properties of Mn(Fe,Ni)(Si,Al) Compounds

Balnude Nuendute¹, Wuliji Hanggai^{1,2}, Hargen Yibole^{1,*}, Bao Tana¹, Ojiyed Tegus^{1,*} and Francois Guillou¹ 

¹ Inner Mongolia Key Laboratory for Physics and Chemistry of Functional Materials, College of Physics and Electronic Information, Inner Mongolia Normal University, 81 Zhaowuda Road, Hohhot 010022, China; nuendute@163.com (B.N.); h.hanggai@tudelft.nl (W.H.); tanaph@imnu.edu.cn (B.T.); francoisguillou@imnu.edu.cn (F.G.)

² FAME Group, Department of Radiation Science & Technology, Delft University of Technology, Mekelweg 15, 2629 JB Delft, The Netherlands

* Correspondence: hyibole@imnu.edu.cn (H.Y.); tegusph@imnu.edu.cn (O.T.)

Abstract: Mn compounds presenting magneto-structural phase transitions are currently intensively studied for their giant magnetocaloric effect; nevertheless, several parameters remain to be further optimized. Here, we explore the Mn(Fe,Ni)(Si,Al) series, which presents two advantages. The Mn content is fixed to unity ensuring a large saturation magnetization, and it is based on non-critical Si and Al elements instead of the more commonly employed Ge. Structural and magnetic properties of MnFe_{0.6}Ni_{0.4}Si_{1-x}Al_x compounds are investigated using powder X-ray diffraction, SEM, EDX, DSC, and magnetic measurements. We demonstrate that a magneto-structural coupling leading to transformation from ferromagnetic with orthorhombic TiNiSi-type structure to a paramagnetic hexagonal Ni₂In-type phase can be realized for 0.06 < x ≤ 0.08. Unfortunately, the first-order transition is relatively broad and incomplete, likely as the result of insufficient sample homogeneity. A comparison between samples synthesized in different conditions (as-cast, quenched from 900 °C, or quenched from 1100 °C) reveals that Mn(Fe,Ni)(Si,Al) samples decompose into a Mn₅Si₃-type phase at intermediate temperatures, preventing the synthesis of high-quality samples by conventional methods such as arc-melting followed by solid-state reaction. By identifying promising MnFe_{0.6}Ni_{0.4}Si_{1-x}Al_x compositions, this study paves the way toward the realization of a giant magnetocaloric effect in these compounds using alternative synthesis techniques.

Keywords: magnetocaloric materials; manganese compounds; phase diagram; magnetic properties



Citation: Nuendute, B.; Hanggai, W.; Yibole, H.; Tana, B.; Tegus, O.; Guillou, F. Drastic Influence of Synthesis Conditions on Structural, Magnetic, and Magnetocaloric Properties of Mn(Fe,Ni)(Si,Al) Compounds. *Crystals* **2022**, *12*, 233. <https://doi.org/10.3390/cryst12020233>

Academic Editor: Jacek Ćwik

Received: 9 December 2021

Accepted: 2 February 2022

Published: 8 February 2022

Publisher's Note: MDPI stays neutral with regard to jurisdictional claims in published maps and institutional affiliations.



Copyright: © 2022 by the authors. Licensee MDPI, Basel, Switzerland. This article is an open access article distributed under the terms and conditions of the Creative Commons Attribution (CC BY) license (<https://creativecommons.org/licenses/by/4.0/>).

1. Introduction

Developing materials with first-order magnetic transitions (FOMTs) is appealing, both in terms of the fundamental interest to unravel the underlying mechanisms and for their potential applications linked to the associated magnetostrictive, magnetoresistive, or magnetocaloric effects (MCEs). In the past two decades, remarkable efforts have been paid at developing materials presenting FOMT near room temperature, as the resulting giant magnetocaloric effect could be used for alternative magnetic cooling or waste heat recovery techniques [1–5]. Various materials families have shown outstanding giant magnetocaloric effect [1–18], among which are MnMX compounds, with M as a transition metal and X a p-block metal or non-metal.

MnMX compounds have raised a peculiar interest, as some of them have the potential to exhibit a coupling between a magnetic ordering transition and a structural transition from orthorhombic TiNiSi type to hexagonal Ni₂In type. Owing to a large structural contribution, the latent heat and giant magnetocaloric effect of such magneto-structural FOMT can be particularly large [19]. A typical example is a MnCoGe compound that

presents a ferromagnetic transition near 340 K and a structural TiNiSi-type (low T.) to Ni₂In-type (high T.) structural transition at ~430 K. When alloyed with a fourth element, the structural transition can be tuned to coincide with the magnetic transition, until achieving a magneto-structurally coupled FOMT with giant magnetocaloric effect and negative thermal expansion [20–23].

Similar magneto-structural transitions were observed in various MnMX compounds. Quaternary or pentanary compounds deriving from MnNiGe or MnNiSi also show large giant-magnetocaloric effect [24,25], including (Mn,Fe)Ni(Si,Ge) or (Mn,Fe)Ni(Si,Al) series with magneto-structural FOMTs [26–29]. However, further optimization of their magnetocaloric effect could be expected.

In ferromagnetic MnMX such as MnCoGe, Mn usually occupies the pyramidal site and carries most of the magnetic moment, nearly 2.8 μ_B /Mn, while Fe, Co, or Ni present significantly lower moments [29,30]. To maximize the magnetic saturation (M_S) and, therefore, the total magnetocaloric effect $\int_0^\infty \Delta S dT = \mu_0 M_S \Delta H$, where ΔS is the isothermal entropy change for a given magnetic field change ΔH , substitutions on Mn should be avoided (neglecting the additional question of the preferential site occupancy). Compounds deriving from Mn₁(Fe,Ni)₁Si₁ with Mn content equal (or larger than 1) will exhibit saturation magnetization larger than those following a (Mn,Fe)₁Ni₁Si₁ chemical formulation and should accordingly be preferred in the search for magnetocaloric materials.

In quaternary Mn(Fe,Ni)Si compounds, a magneto-structural coupling could not be realized. A recent study on Mn(Fe,Ni)(Si,Ge) revealed that magneto-structural coupling could be achieved by Ge for Si substitutions [31]. While promising, these compounds are not ideal, as Ge is a scarce and expensive element of critical supply. We, therefore, explore in the present study the possibility of realizing a magneto-structural coupling by Al for Si substitutions in Mn(Fe,Ni)Si_{1-x}Al_x compounds.

2. Materials and Methods

Elemental Mn, Fe, Ni, Si, Al pieces with a purity of 99.9% and above were used as starting materials. The samples (5 to 10 g) were arc melted in a WK Series Vacuum Arc Melting (China) furnace in ~500 mbar Ar atmosphere purified using a Ti getter. The melting is repeated four times while flipping the button at each iteration. For annealing, sample pieces were cut from the as-cast buttons and sealed in quartz tubes backfilled with ~200 mbar Ar. Different heat treatment durations and temperatures were attempted. In this manuscript, we focus on a comparison of (1) as-cast samples; (2) samples annealed at 1100 °C for 80 h, followed by quenching in water; (3) annealed at 900 °C for 80 h, followed by quenching in water. For the latter heat treatment, we note that quenching or slow cooling results in little to no difference in structural and magnetic properties.

Powder X-ray diffraction (XRD) was carried out at room temperature on an Empyrean Panalytical diffractometer (Almelo, Netherlands) employing Cu K α radiation. Phase identification was carried out using the Expert HighScore software, and Rietveld refinements were performed using the FullProf software [32]. Local chemical compositions and surface morphology were established using a Hitachi (Chiyoda, Tokyo, Japan) TM3030 Plus scanning electron microscope (SEM) equipped with an energy-dispersive spectrometer (EDX).

Differential scanning calorimetry (DSC) experiments were carried out on a TA Instruments DSC 2500 (New Castle, DE, USA), equipped with a liquid nitrogen pumping system and using Al crucibles. Magnetization measurements were carried out on samples of approximately 10 mg in a Quantum Design (San Diego, CA, USA) Versalab system, equipped with a vibrating sample magnetometer option.

3. Results and Discussion

3.1. Orthorhombic-to-Hexagonal Transition in MnFe_{0.6}Ni_{0.4}Si_{1-x}Al_x Compounds

Figure 1 shows the room-temperature XRD patterns of MnFe_{0.6}Ni_{0.4}Si_{1-x}Al_x compounds (quenched from 1100 °C) and Table 1 lists their refined lattice parameters, unit

cell volumes, and phase fractions. All noticeable diffraction peaks can be indexed in the TiNiSi-type orthorhombic structure (space group $Pnma$) or in the Ni₂In-type hexagonal structure (space group $P6_3/mmc$). Samples with $x < 0.06$ crystallize in the orthorhombic structure, while the sample $x = 0.08$ crystallizes in the hexagonal structure. At room temperature, the sample $x = 0.06$ presents a phase coexistence of TiNiSi-type and Ni₂In-type structures. Within the stability range of the orthorhombic structure, Al substitutions do not lead to a significant evolution of the unit cell volume, while the latter slightly decreases from $x = 0.06$ to 0.08 for the hexagonal phase. More importantly, using the conversion $V_{ortho} = 2V_{hexa.}$, the difference in cell volume between orthorhombic to hexagonal structures in the mixed-phase sample $x = 0.06$ is large and negative $\Delta V/V \approx -3.3\%$. This is in line with former reports indicating that the TiNiSi-to-Ni₂In-type transformation as a function of chemical composition or induced by temperature results in a large negative cell volume change [20].

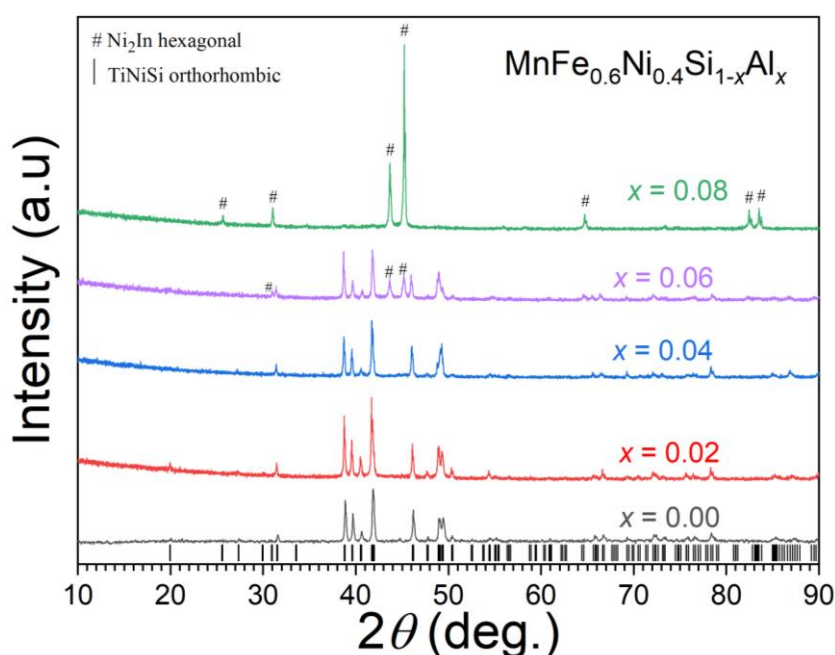


Figure 1. X-ray diffraction patterns at room temperature for $MnFe_{0.6}Ni_{0.4}Si_{1-x}Al_x$ compounds (quenched from 1100 °C). Vertical lines and octothorpes mark out the reflections from orthorhombic TiNiSi-type and hexagonal Ni₂In-type structures, respectively.

Table 1. Refined room temperature lattice parameters, unit cell volume, and phase fractions for $MnFe_{0.6}Ni_{0.4}Si_{1-x}Al_x$ compounds (the statistical uncertainty on the last digit is indicated in brackets).

x	Orthorhombic TiNiSi-Type					Hexagonal Ni ₂ In-Type		
	a (Å)	b (Å)	c (Å)	V (Å ³)	wt.%	a (Å)	c (Å)	V (Å ³)
0.00	5.7825 (9)	3.6930 (5)	6.9730 (9)	148.91 (5)	100			
0.02	5.7812 (5)	3.6926 (3)	6.9710 (5)	148.82 (3)	100			
0.04	5.7649 (7)	3.7010 (4)	6.9756 (8)	148.83 (3)	100			
0.06	5.7398 (6)	3.7157 (4)	6.9798 (7)	148.86 (3)	73.6 (8)	4.0115 (5)	5.1640 (9)	71.96 (2)
0.08						4.0050 (3)	5.1588 (5)	71.67 (1)

Figure 2 shows the magnetization as a function of temperature for $MnFe_{0.6}Ni_{0.4}Si_{1-x}Al_x$ compounds. The transition temperatures are taken as dM/dT extrema. For $0 \leq x \leq 0.04$ compounds, orthorhombic at room temperature, the only significant feature is the

ferromagnetic–paramagnetic transition occurring in the range of 292–302 K. For some samples, an additional wave-like anomaly can be distinguished at low temperatures (in the range 50–100 K) and low magnetic fields; however, as this minor feature becomes indistinguishable at higher magnetic fields, it is disregarded. The absence of thermal hysteresis and the swift broadening of the ferromagnetic transition when higher magnetic fields are applied (not shown) indicate that the ferromagnetic transition is of second-order in this compositional range. For the mixed-phase sample $x = 0.06$, two magnetic anomalies can be distinguished near 285 K and near 145 K, attributed to the ferromagnetic transitions of the orthorhombic fraction and of the hexagonal fraction, respectively. Since hexagonal Ni_2In -to- TiNiSi -type structural transition may occur as a function of temperature and that such transition is usually first-order with a large thermal hysteresis [20–24], the absence of thermal hysteresis in $x = 0.06$ suggests that no hexagonal-to-orthorhombic transformation occurs near 285 K or 145 K in this sample. At high Al content, e.g., hexagonal $x = 0.08$, one is left with a single ferromagnetic transition with a Curie temperature (T_C) of 148 K upon cooling. Interestingly, the subsequent measurement upon heating reveals a large thermal hysteresis occurring in part of the samples. This indicates that a fraction of the sample experiences a magneto-structural para.(hexagonal) to ferro.(orthorhombic) FOMTs typical of this family of MnMX compounds [20–24]. The magneto-structural transition appears relatively broad and does not occur in the full sample. This might originate from chemical disorder promoted by the high-temperature annealing and from local compositional inhomogeneities but smaller than those detectable from the brightness, contrast, and intensity conditions of our SEM/EDX measurements.

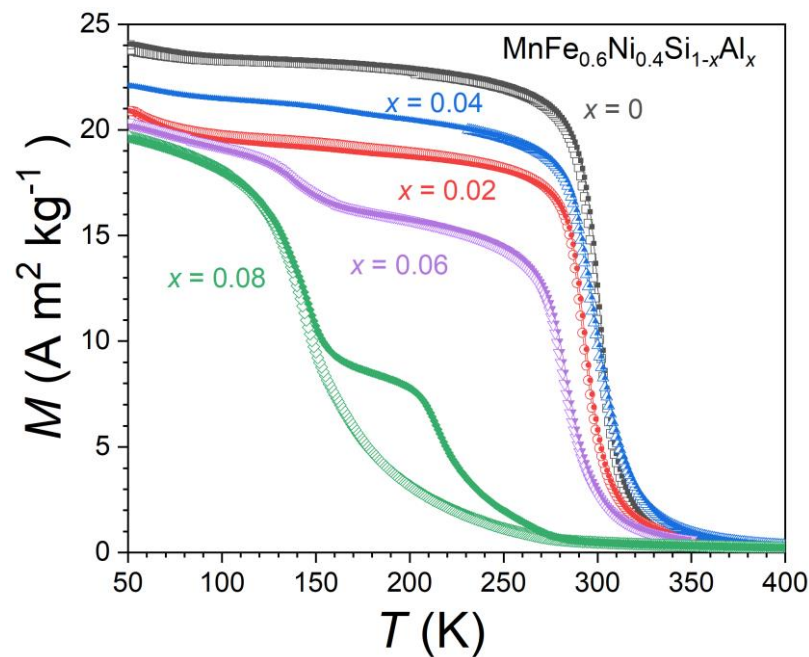


Figure 2. $M(T)$ curves for $\text{MnFe}_{0.6}\text{Ni}_{0.4}\text{Si}_{1-x}\text{Al}_x$ compounds measured upon heating (full symbols) and cooling (open symbols) in an applied field of $\mu_0 H = 0.05$ T.

Figure 3 presents DSC measurements on $\text{MnFe}_{0.6}\text{Ni}_{0.4}\text{Si}_{1-x}\text{Al}_x$ compounds. The thermogram for $x = 0.04$ presents two anomalies—a weak kink at $T_C \approx 295$ K typical of a second-order transition and a stronger anomaly with finite latent heat and thermal hysteresis that we attribute to the structural TiNiSi -to- Ni_2In -type transition at $T_{tr} = 530$ K (upon heating). When increasing the Al content, the most pronounced evolution is the swift decrease in the structural transition temperature T_{tr} . For $x = 0.08$, only one thermal anomaly is observed at $T_{tr} = 210$ K (upon heating). Integrating the heat flow peak after subtraction of

a linear background allows one to estimate the entropy change of the transition $\Delta S_{tr} = L/T_C \approx 12 \text{ J kg}^{-1} \text{ K}^{-1}$ due to the latent heat (L) of the FOMT in $x = 0.08$.

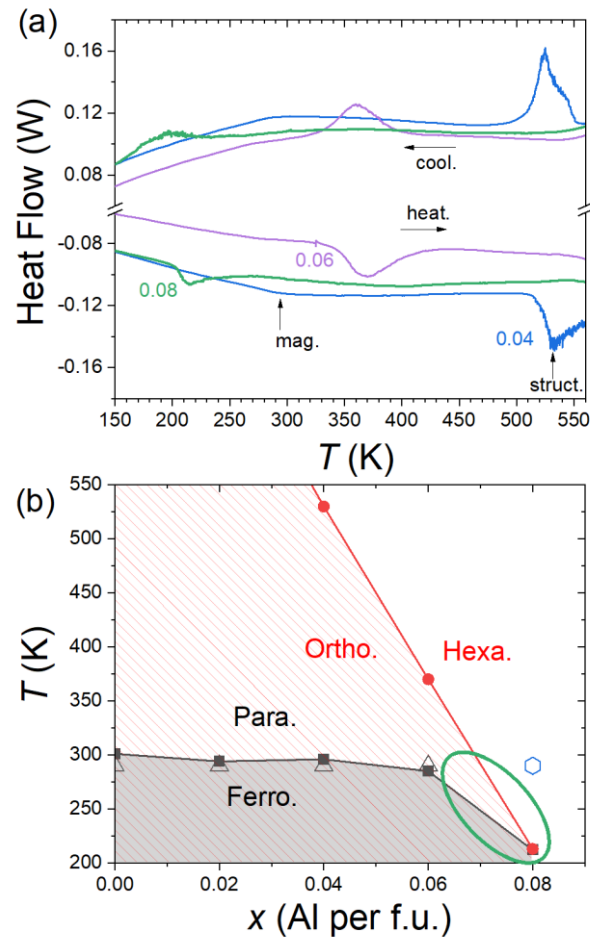


Figure 3. (a) DSC measurements of $\text{MnFe}_{0.6}\text{Ni}_{0.4}\text{Si}_{1-x}\text{Al}_x$ compounds carried out at 10 K min^{-1} upon heating (lower set of curves) and cooling (upper set of curves). The arrows illustrate the location of the magnetic (mag.) and structural (struct.) transitions for $x = 0.04$; (b) structural and magnetic phase diagram displaying the Curie temperatures determined from $M(T)$ measurements at low magnetic fields (filled squares), the structural ortho.–hexa. transition (filled circles) determined from DSC measurements and the main structure type at room temperature established by XRD (open triangles for TiNiSi type, open hexagon for Ni₂In type). The circle highlights the range where a magneto-structural coupling is expected.

A summarizing phase diagram regrouping information from room temperature XRD data, magnetization, and DSC measurements for $\text{MnFe}_{0.6}\text{Ni}_{0.4}\text{Si}_{1-x}\text{Al}_x$ compounds is shown in Figure 3b. The structural T_{tr} transition temperature decreases particularly quickly with Al substitution, while in the meantime, the T_C values of orthorhombic compounds show no significant evolution. As a result, $T_{tr}(x)$ and $T_C(x)$ transition lines merge around $0.06 < x \leq 0.08$, corresponding to the range in which a magneto-structural coupling occurs, leading to the appearance of a first-order ferromagnetic orthorhombic-to-hexagonal paramagnetic transition. We note that the appearance of a coupled magneto-structural transition leads to a swift decrease in T_C , which is typical of the phase diagrams of closely related MnNiGe compounds [24]. $\text{MnFe}_{0.6}\text{Ni}_{0.4}\text{Si}_{1-x}\text{Al}_x$ $0.06 < x \leq 0.08$ compounds with magneto-structural coupling are expected to present a giant magnetocaloric effect. However, the broadness of the first-order transition for $x = 0.08$ will limit the interest of the present samples as the magnetocaloric effect will be spread over a large temperature window, resulting in reduced entropy change ΔS or temperature change ΔT_{ad} . The next section is, therefore, devoted to a

more detailed investigation of the influence of the synthesis conditions, in view of defining pathways to sharpen the FOMT.

3.2. Influence of Synthesis Conditions on Crystal Structure and Properties of $\text{MnFe}_{0.53}\text{Ni}_{0.47}\text{Si}_{0.94}\text{Al}_{0.06}$

We attempted to sharpen the magneto-structural transition by optimizing the annealing conditions. Figure 4 shows the room-temperature XRD patterns of three $\text{MnFe}_{0.53}\text{Ni}_{0.47}\text{Si}_{0.94}\text{Al}_{0.06}$ samples synthesized by using different heat treatments. The Ni content was slightly increased in comparison with the samples from Section 3.1, with the aim to increase the magnetic ordering temperature. The Al content was selected as $x = 0.06$, which corresponds to the compositional range where structural and magnetic transition temperatures coincide for this sample. From high-temperature DSC and annealing experiments, the melting point of $\text{MnFe}_{0.53}\text{Ni}_{0.47}\text{Si}_{0.94}\text{Al}_{0.06}$ was found to be around 1145 °C. In order to promote homogeneity of the sample by solid-state diffusion at a reasonable time scale, two synthesis conditions were considered in addition to the as-cast sample—quenched from 900 °C and quenched from 1100 °C. Drastic differences can be observed between the diffraction patterns from the samples prepared by different synthesis conditions. The as-cast sample shows a phase coexistence of orthorhombic TiNiSi-type (approximately 55 mol.% from XRD refinement) and hexagonal Ni_2In -type phases. Heat treatment at 1100 °C significantly affects the structure, as this sample now presents a nearly single Ni_2In -type phase (tiny diffraction peaks can be distinguished corresponding to approximately 6 mol.% of orthorhombic phase). In contrast to as-cast or 1100 °C heat treatments, the sample heat-treated and quenched from 900 °C reveals the appearance of another structure, leading to the coexistence of three phases: orthorhombic TiNiSi-type, hexagonal Ni_2In -type, and a significant fraction of an additional hexagonal phase with a structure very similar to that of Mn_5Si_3 (space group $P6_3/mcm$, phase fraction roughly estimated to 47 mol.%). From XRD, the three synthesis conditions, therefore, lead to three samples with drastically different crystal structures.

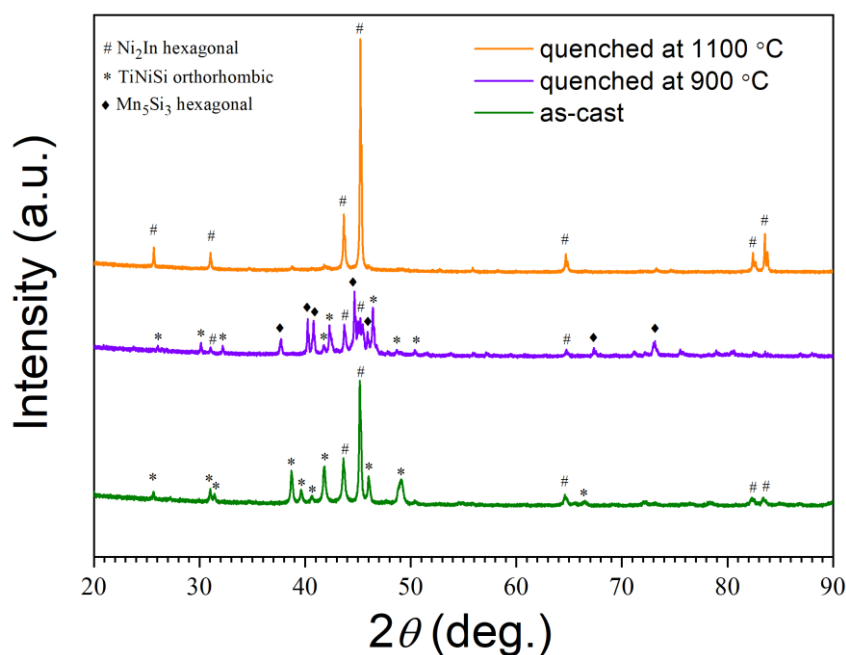


Figure 4. Room-temperature X-ray diffraction patterns of $\text{MnFe}_{0.53}\text{Ni}_{0.47}\text{Si}_{0.94}\text{Al}_{0.06}$ samples synthesized using different conditions.

In order to grasp more details on the structure and microstructure of $\text{MnFe}_{0.53}\text{Ni}_{0.47}\text{Si}_{0.94}\text{Al}_{0.06}$ compounds, SEM imaging coupled to EDX chemical analyses

were carried out (Figure 5). No elemental contrast nor secondary phases could be distinguished for as-cast or quenched at 1100 °C samples. Their effective chemical compositions estimated from EDX are $\text{Mn}_{0.97}\text{Fe}_{0.53}\text{Ni}_{0.45}\text{Si}_{0.95}\text{Al}_{0.07}$ and $\text{Mn}_{0.99}\text{Fe}_{0.52}\text{Ni}_{0.49}\text{Si}_{0.95}\text{Al}_{0.07}$, respectively, which is in reasonable agreement with their nominal composition (the statistical uncertainty on chemical formula from EDX analyses is in the range 0.03–0.06 depending on elements). For the as-cast sample showing from XRD the coexistence of significant fractions of hexagonal Ni_2In -type structure and orthorhombic TiNiSi -type structure, no elemental contrast could be detected. This indicates that these two phases have very similar effective compositions, and their coexistence is due to the structural transition between them taking place near room temperature (Figure 6). In stark contrast, the sample annealed at 900 °C shows a lamellar-like development of large secondary phase content with clear elemental contrast. The bright phase (heavier average atomic number in backscattered electron detection) corresponds to a metal:metalloid ratio close to 2:1 but with an effective composition of $\text{Mn}_{1.06}\text{Fe}_{0.56}\text{Ni}_{0.38}\text{Si}_{0.93}\text{Al}_{0.07}$ significantly different from the nominal one. The dark spot presents a reduced metal:metalloid ratio $n(\text{Mn} + \text{Fe} + \text{Ni}) : n(\text{Si} + \text{Al}) \approx 1.25$ or $n(\text{Mn} + \text{Fe} + \text{Ni} + \text{Al}) : n(\text{Si}) = 1.63$, which would be close to that of the Mn_5Si_3 -type hexagonal structure detected on the XRD diffractogram. We note that the secondary phase with reduced metal:metalloid ratio represents nearly half the sample on SEM imaging, which is in agreement with the large fraction of Mn_5Si_3 -type phase detected in XRD. Similar to the case of the as-cast sample, no elemental contrast is expected between hexagonal Ni_2In -type structure and orthorhombic TiNiSi -type structure in the sample annealed at 900 °C, as only two different phases are observed in SEM/EDX experiments, while three were detected from XRD.

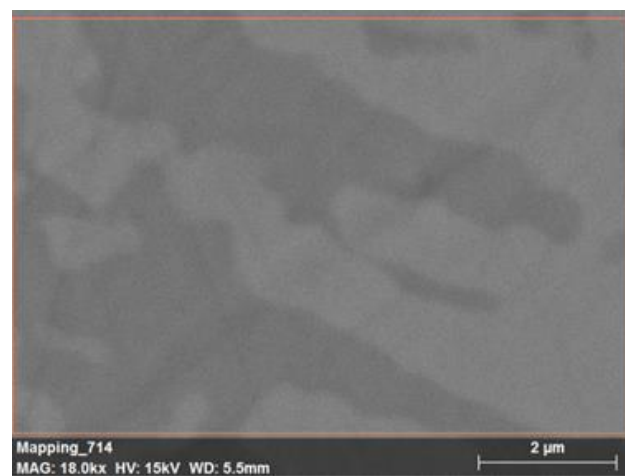


Figure 5. SEM imaging used for EDX analyses of the $\text{MnFe}_{0.53}\text{Ni}_{0.47}\text{Si}_{0.94}\text{Al}_{0.06}$ sample quenched from 900 °C.

Figure 6 shows the magnetization data of $\text{MnFe}_{0.53}\text{Ni}_{0.47}\text{Si}_{0.94}\text{Al}_{0.06}$ compounds. As-cast or quenched 1100 °C samples exhibit a ferromagnetic behavior, while the sample quenched from 900 °C does not show any signs of ferromagnetic ordering. The as-cast sample presents a first-order ferromagnetic transition centered around 310 K with finite hysteresis. However, this transition is particularly broad. The sample quenched at 1100 °C shows a relatively sharper ferromagnetic transition but at a lower temperature of $T_C = 190$ K upon heating and a sizable thermal hysteresis of 23 K. The presence of a sizable thermal hysteresis at T_C is distinctive of a first-order magnetic transition. In addition, complementary DSC measurements show a broad yet rather symmetrical latent heat peak further confirming the occurrence of a FOMT and whose integration leads to an estimate of the transition entropy of $\Delta S_{tr} \approx 11 \text{ J kg}^{-1} \text{ K}^{-1}$. The saturation magnetization of the sample quenched at 1100 °C is lower than the as-cast sample, which may be ascribed to non-complete phase transition toward the orthorhombic ferromagnetic state. On $M(T)$ or $M(H)$ curves, the mag-

netization of the sample quenched from 900 °C is much lower than that of the samples from other synthesis methods and does not exhibit signs of ferromagnetism on the $M(H)$ curve at 50 K. This can be ascribed to the unwanted Mn_5Si_3 -type phase, which forms most of the sample quenched from 900 °C and is antiferromagnetic at low Fe content [33]. In addition, the effective composition of the targeted MnMX compound is affected by the decomposition occurring at 900 °C. This appears to trigger a disappearance of the ferromagnetism. On the other hand, the saturation magnetization of as-cast $\text{MnFe}_{0.53}\text{Ni}_{0.47}\text{Si}_{0.94}\text{Al}_{0.06}$ reaches $114 \text{ A m}^2 \text{ kg}^{-1}$, i.e., $2.86 \mu_B/\text{f.u.}$ This value turns out to be significantly larger than the values reported for MnMX compounds for which chemical substitutions are made at the expense of Mn, e.g., larger than the $\sim 80 \text{ A m}^2 \text{ kg}^{-1}$ obtained in $\text{Mn}_{1-x}\text{Fe}_x\text{NiGe}$ [24] or larger than the $\sim 75 \text{ A m}^2 \text{ kg}^{-1}$ reached in $\text{Mn}_{0.5}\text{Fe}_{0.5}\text{NiSi}_{1-x}\text{Al}_x$ [29]. This brings support to our initial hypothesis that MnMX compounds with a Mn content equal to or larger than unity exhibit larger saturation magnetization.

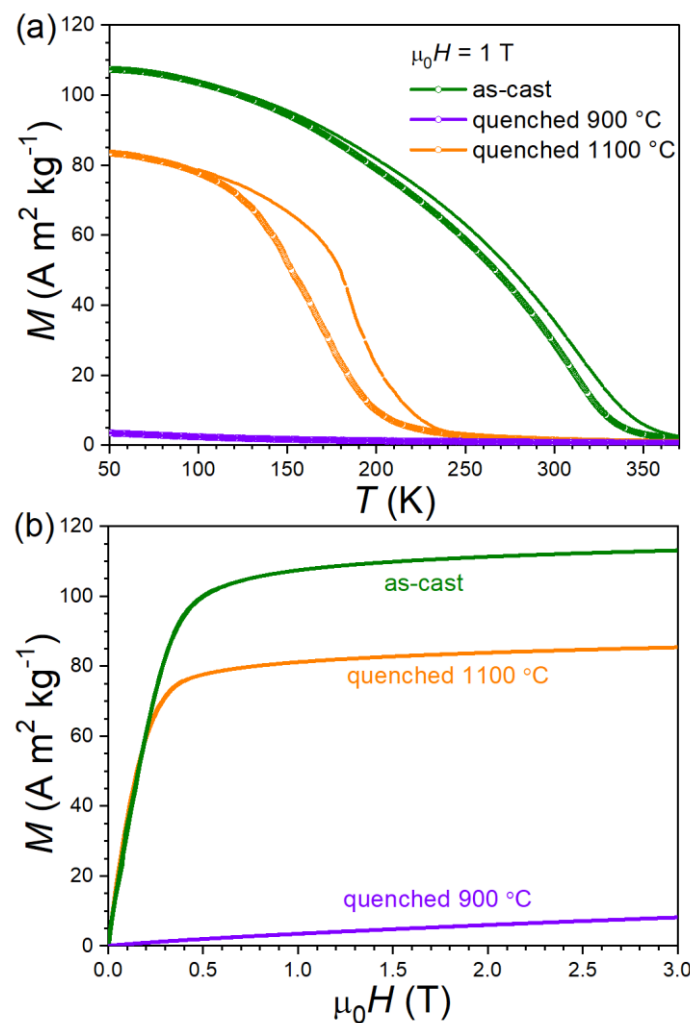


Figure 6. Magnetization of $\text{MnFe}_{0.53}\text{Ni}_{0.47}\text{Si}_{0.94}\text{Al}_{0.06}$ synthesized using different conditions: (a) as a function of temperature upon heating (line) and cooling (symbols); (b) isothermal magnetization curves recorded at $T = 50 \text{ K}$.

Magnetization-versus-temperature curves were recorded in different external magnetic fields in order to calculate the isothermal entropy change (ΔS) via the Maxwell relation $\Delta S = \int_0^{B'} \left(\frac{\partial M}{\partial T}\right)_B dB$. Figure 7 presents a set of $M(T)$ curves and the corresponding magnetocaloric effect (ΔS) for the $\text{MnFe}_{0.53}\text{Ni}_{0.47}\text{Si}_{0.94}\text{Al}_{0.06}$ sample quenched from 1100 °C. First, when increasing the applied magnetic field, we observe that the magnetization jump of

the ferromagnetic transition experiences a shift to a higher temperature of approximately +12 K for 3 T ($dT_C/\mu_0dH \approx 4 \text{ K T}^{-1}$) and broadens, which is typical of a ferromagnetic FOMT. The isothermal entropy change curve $\Delta S(T)$ reflects the broadness of the FOMT, the latter also manifests itself by a splitting of the ΔS peak into several substructures. A maximal magnetocaloric effect of $3.8 \text{ J kg}^{-1} \text{ K}^{-1}$ is reached for a magnetic field change of 3 T. For a field change of 2 T, the magnetocaloric effect reaches $2.7 \text{ J kg}^{-1} \text{ K}^{-1}$ and is spread over a large temperature window, with a full width at half maximum of $\sim 50 \text{ K}$.

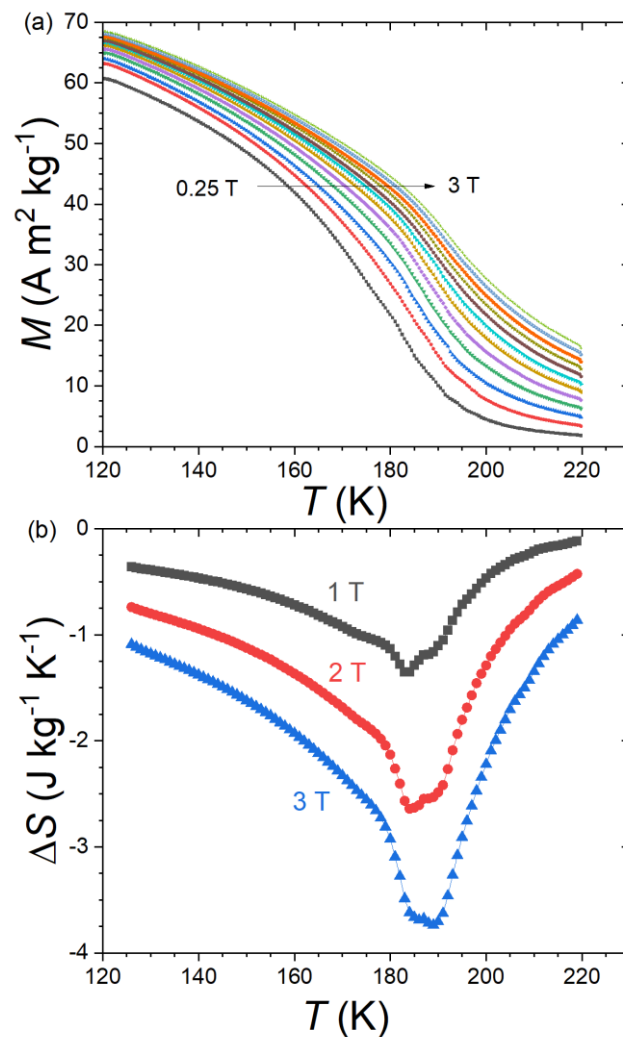


Figure 7. Magnetocaloric effect of $\text{MnFe}_{0.53}\text{Ni}_{0.47}\text{Si}_{0.94}\text{Al}_{0.06}$ quenched from $1100 \text{ }^\circ\text{C}$: (a) $M(T)$ curves recorded upon heating in different magnetic fields (heating rate = 1 K min^{-1}); (b) isothermal entropy change calculated from $M(T)$ curves upon heating.

Ultimately, while $\text{Mn}(\text{Ni,Fe})\text{Si}_{1-x}\text{Al}_x$ compounds can be tuned to present a magneto-structural coupling, the amplitude of their magnetocaloric effect is closer to that of second-order transitions rather than the giant MCE usual to MnMX compounds. The primary reason for this low ΔS is the broadness of the transition. Schematic descriptions of the isothermal entropy change at FOMTs leads to an expression $\Delta S(H) = (\Delta S_{\text{tr}} \times \Delta H \times (dT_C/dH))/\delta T_{\text{tr}}$, where (dT_C/dH) is the shift of the transition due to the application of a magnetic field and δT_{tr} is the transition width [34]. In the present sample, ΔS_{tr} and (dT_C/dH) are sizable, as large as in usual giant MCE materials [34]. However, the width of the transition (δT_{tr}) is also particularly large, which results in a reduced magnetocaloric effect. The broadness of the FOMT itself is born from the difficulty to synthesize high-quality samples due to the stability of an unwanted Mn_5Si_3 -type secondary phase in the

intermediate temperature range around 900 °C. This is particularly unfortunate, as MnMX compounds exhibiting the sharpest FOMT and, therefore, highest ΔS maxima are precisely synthesized by solid-state reaction at 800–900 °C [24,29].

4. Conclusions

The structural and magnetic phase diagrams of $\text{MnFe}_{0.6}\text{Ni}_{0.4}\text{Si}_{1-x}\text{Al}_x$ compounds were established using powder X-ray diffraction, DSC, and magnetic measurements. A magnetostructural coupling leading to ferromagnetic TiNiSi-type orthorhombic-to-paramagnetic Ni_2In -type hexagonal structure can be realized for $0.06 < x \leq 0.08$. These compounds with Mn content fixed to unity present a larger saturation magnetization than quaternary or pentanary MnMX compounds in which substitutions are made at the expense of Mn. Samples synthesized in different conditions (as-cast, quenched from 900 °C, or quenched from 1100 °C) were compared. From XRD, SEM, and EDX, it is found that $\text{MnFe}_{0.53}\text{Ni}_{0.47}\text{Si}_{0.94}\text{Al}_{0.06}$ samples decompose into a Mn_5Si_3 -type phase at intermediate temperatures (around 900 °C), which prevents the synthesis of high-quality samples with sharp FOMT by conventional methods such as arc-melting followed by solid-state reaction. In order to reach a larger giant magnetocaloric effect, alternative synthesis techniques, in particular those leading to reduced solid-state reaction duration, should be investigated.

Author Contributions: Conceptualization, B.N. and O.T.; investigation, B.N., W.H. and B.T.; writing—original draft preparation, B.N.; writing—review and editing, F.G.; visualization, B.N. and F.G.; supervision, O.T., H.Y. and F.G.; project administration, H.Y.; funding acquisition, H.Y. All authors have read and agreed to the published version of the manuscript.

Funding: This research was funded by the National Natural Science Foundation of China (Grant Nos. 11904188, 51961033, and 52150610486), the Inner Mongolia Autonomous Region (Grant Nos. NJZY20025 and NJYT-20-A17), and the Inner Mongolia Normal University (Grant Nos. 2018YJRC002 and 2018YJRC003).

Institutional Review Board Statement: Not applicable.

Informed Consent Statement: Not applicable.

Data Availability Statement: The data presented in this study are available on request from the authors.

Conflicts of Interest: The authors declare no conflict of interest.

References

1. Gschneidner, K.A., Jr.; Pecharsky, V.K.; Tsoko, A.O. Recent developments in magnetocaloric materials. *Rep. Prog. Phys.* **2005**, *68*, 1479. [[CrossRef](#)]
2. Gutfleisch, O.; Willard, M.A.; Brück, E.; Chen, C.H.; Sankar, S.G.; Ping Liu, J. Magnetic Materials and Devices for the 21st Century: Stronger, Lighter, and More Energy Efficient. *Adv. Mater.* **2011**, *23*, 821–842. [[CrossRef](#)] [[PubMed](#)]
3. Smith, A.; Bahl, C.R.H.; Bjørk, R.; Engelbrecht, K.; Nielsen, K.K.; Pryds, N. Materials Challenges for High Performance Magnetocaloric Refrigeration Devices. *Adv. Energy Mater.* **2012**, *2*, 1288–1318. [[CrossRef](#)]
4. Balli, M.; Jandl, S.; Fournier, P.; Kedous-Lebouc, A. Advanced materials for magnetic cooling: Fundamentals and practical aspects. *Appl. Phys. Rev.* **2017**, *4*, 021305. [[CrossRef](#)]
5. Kitanovski, A. Energy Applications of Magnetocaloric Materials. *Adv. Energy Mater.* **2020**, *10*, 1903741. [[CrossRef](#)]
6. Hu, F.X.; Shen, B.G.; Sun, J.R.; Cheng, Z.H.; Rao, G.H.; Zhang, X.X. Influence of negative lattice expansion and metamagnetic transition on magnetic entropy change in the compound $\text{LaFe}_{11.4}\text{Si}_{1.6}$. *Appl. Phys. Lett.* **2001**, *78*, 3675–3677. [[CrossRef](#)]
7. Fujita, A.; Fujieda, S.; Fukamichi, K.; Mitamura, H.; Goto, T. Itinerant-electron metamagnetic transition and large magnetovolume effects in $\text{La}(\text{Fe}_x\text{Si}_{1-x})_{13}$ compounds. *Phys. Rev. B* **2001**, *65*, 014410. [[CrossRef](#)]
8. Krenke, T.; Duman, E.; Acet, M.; Wassermann, E.F.; Moya, X.; Mañosa, L.; Planes, A. Inverse magnetocaloric effect in ferromagnetic Ni-Mn-Sn alloys. *Nat. Mater.* **2005**, *4*, 450–454. [[CrossRef](#)]
9. Li, Y.; Zeng, Q.Q.; Wei, Z.Y.; Liu, E.K.; Han, X.L.; Du, Z.W.; Li, L.W.; Xi, X.K.; Wang, W.H.; Wang, S.G.; et al. An efficient scheme to tailor the magnetostructural transitions by staged quenching and cyclical ageing in hexagonal martensitic alloys. *Acta Mater.* **2019**, *174*, 289–299. [[CrossRef](#)]
10. Li, L.W.; Xu, P.; Ye, S.K.; Li, Y.; Liu, G.D.; Huo, D.X.; Yan, M. Magnetic properties and excellent cryogenic magnetocaloric performances in B-site ordered $\text{RE}_2\text{ZnMnO}_6$ (RE = Gd, Dy and Ho) perovskites. *Acta Mater.* **2020**, *194*, 354–365. [[CrossRef](#)]

11. Wu, B.B.; Zhang, Y.K.; Guo, D.; Wang, J.; Ren, Z.M. Structure, magnetic properties and cryogenic magneto-caloric effect (MCE) in RE₂FeAlO₆ (RE = Gd, Dy, Ho) oxides. *Ceram. Int.* **2021**, *47*, 6290–6297. [[CrossRef](#)]
12. Wang, Y.M.; Guo, D.; Wu, B.B.; Geng, S.H.; Zhang, Y.K. Magnetocaloric effect and refrigeration performance in RE₆₀Co₂₀Ni₂₀ (RE = Ho and Er) amorphous ribbons. *J. Magn. Magn. Mater.* **2020**, *498*, 166179. [[CrossRef](#)]
13. Ma, Z.P.; Dong, X.S.; Zhang, Z.Q.; Li, L.W. Achievement of promising cryogenic magnetocaloric performances in La_{1-x}Pr_xFe₁₂B₆ compounds. *J. Mater. Sci. Technol.* **2021**, *92*, 138–142. [[CrossRef](#)]
14. Zou, J.D.; Shen, B.G.; Gao, B.; Shen, J.; Sun, J.R. The magnetocaloric effect of LaFe_{11.6}Si_{1.4}, La_{0.8}Nd_{0.2}Fe_{11.5}Si_{1.5}, and Ni₄₃Mn₄₆Sn₁₁ compounds in the vicinity of the first-order phase transition. *Adv. Mater.* **2009**, *21*, 693–696. [[CrossRef](#)]
15. Shen, B.G.; Sun, J.R.; Hu, F.X.; Zhang, H.W.; Cheng, Z.H. Recent progress in exploring magnetocaloric materials. *Adv. Mater.* **2009**, *21*, 4545–4564. [[CrossRef](#)]
16. Zhang, H.; Liu, J.; Zhang, M.; Shao, Y.; Li, Y.; Yan, A. LaFe_{11.6}Si_{1.4}Hy/Sn magnetocaloric composites by hot pressing. *Scr. Mater.* **2016**, *120*, 58–61.
17. Zhang, H.; Li, Y.; Liu, E.; Ke, Y.; Jin, J.; Long, Y.; Shen, B.G. Giant rotating magnetocaloric effect induced by highly texturing in polycrystalline DyNiSi compound. *Sci. Rep.* **2015**, *5*, 11929. [[CrossRef](#)]
18. Ćwik, J.; Koshkid'ko, Y.; Małecka, M.; Weise, B.; Krautz, M.; Mikhailova, A.; Kolchugina, N. Magnetocaloric prospects of mutual substitutions of rare-earth elements in pseudobinary Tb_{1-x}Ho_xNi₂ compositions (x = 0.25–0.75). *J. Alloys Compd.* **2021**, *886*, 161295. [[CrossRef](#)]
19. Gschneidner, K.A., Jr.; Mudryk, Y.; Pecharsky, V.K. On the nature of the magnetocaloric effect of the first-order magneto-structural transition. *Scr. Mater.* **2012**, *67*, 572–577. [[CrossRef](#)]
20. Johnson, V. Diffusionless orthorhombic to hexagonal transitions in ternary silicides and germanides. *Inorg. Chem.* **1975**, *14*, 1117–1120. [[CrossRef](#)]
21. Trung, N.T.; Zhang, L.; Caron, L.; Buschow, K.H.J.; Brück, E. Giant magnetocaloric effects by tailoring the phase transitions. *Appl. Phys. Lett.* **2010**, *96*, 172504. [[CrossRef](#)]
22. Liu, J.; Skokov, K.; Gutfleisch, O. Magnetostructural transition and adiabatic temperature change in Mn–Co–Ge magnetic refrigerants. *Scr. Mater.* **2012**, *66*, 642–645. [[CrossRef](#)]
23. Miao, X.; Gong, Y.; Caron, L.; You, Y.; Xu, G.; Sheptyakov, D.; Manuel, P.; Qian, F.; Zhang, Y.; Xu, F.; et al. Switching the magnetostructural coupling in MnCoGe-based magnetocaloric materials. *Phys. Rev. Materials* **2020**, *4*, 104407. [[CrossRef](#)]
24. Liu, E.; Wang, W.; Feng, L.; Zhu, W.; Li, G.; Chen, J.; Zhang, H.; Wu, G.; Jiang, C.; Xu, H.; et al. Stable magnetostructural coupling with tunable magnetoresponse effects in hexagonal ferromagnets. *Nat Commun.* **2012**, *3*, 873. [[CrossRef](#)]
25. Taubel, A.; Gottschall, T.; Fries, M.; Faske, T.; Skokov, K.P.; Gutfleisch, O. Influence of magnetic field, chemical pressure and hydrostatic pressure on the structural and magnetocaloric properties of the Mn–Ni–Ge system. *J. Phys. D Appl. Phys.* **2017**, *50*, 464005. [[CrossRef](#)]
26. Dutta, P.; Pramanick, S.; Chattopadhyay, S.; Das, D.; Chatterjee, S. Observation of colossal magnetocaloric effect and its dependence on applied hydrostatic pressure in thermally cycled Mn_{0.53}Fe_{0.47}NiSi_{0.53}Ge_{0.47} alloy. *J. Alloys Compd.* **2018**, *735*, 2087–2091. [[CrossRef](#)]
27. Liu, K.; Ma, S.C.; Ma, C.C.; Yang, S.; Ge, Q.; Han, X.Q.; Yu, K.; Song, Y.; Zhang, Z.S.; Chen, C.C.; et al. Tuning the magnetostructural transformation by wheel speed in Mn–Fe–Ni–Ge–Si alloy ribbons. *J. Alloys Compd.* **2018**, *746*, 503–508. [[CrossRef](#)]
28. Zhang, C.L.; Shi, H.F.; Nie, Y.G.; Ye, E.J.; Han, Z.D.; Wang, D.H. Thermal-cycling-dependent magnetostructural transitions in a Ge-free system Mn_{0.5}Fe_{0.5}Ni(Si,Al). *Appl. Phys. Lett.* **2014**, *105*, 242403. [[CrossRef](#)]
29. Biswas, A.; Pathak, A.K.; Zharkevich, N.A.; Liu, X.; Mudryk, Y.; Balema, V.; Johnson, D.D.; Pecharsky, V.K. Designed materials with the giant magnetocaloric effect near room temperature. *Acta Mater.* **2019**, *180*, 341–348. [[CrossRef](#)]
30. Nizioł, S.; Bombik, A.; Bazela, W.; Szytuła, A.; Fruchart, D. Crystal and magnetic structure of Co_xNi_{1-x}MnGe system. *J. Magn. Magn. Mater.* **1982**, *27*, 281–292. [[CrossRef](#)]
31. Hanggai, W.; Tegus, O.; Yibole, H.; Guillou, F. Structural and magnetic phase diagrams of MnFe_{0.6}Ni_{0.4}(Si,Ge) alloys and their giant magnetocaloric effect probed by heat capacity measurements. *J. Magn. Magn. Mater.* **2020**, *494*, 165785. [[CrossRef](#)]
32. Rodríguez-Carvajal, J. Recent advances in magnetic structure determination by neutron powder diffraction. *Physica B* **1993**, *192*, 55–69. [[CrossRef](#)]
33. Songlin, D.; Tegus, O.; Brück, E.; Klaasse, J.C.P.; de Boer, F.R.; Buschow, K.H.J. Magnetic phase transition and magnetocaloric effect in Mn_{5-x}Fe_xSi₃. *J. Alloys Compd.* **2002**, *334*, 249. [[CrossRef](#)]
34. Guillou, F.; Yibole, H.; Kamantsev, A.; Porcari, G.; Ćwik, J.; Koledov, V.; van Dijk, N.H.; Brück, E. Field Dependence of the Magnetocaloric Effect in MnFe (P,Si) Materials. *IEEE Trans. Magn.* **2015**, *51*, 2503904. [[CrossRef](#)]